Flow, Turbulence and Combustion (2025) 115:1631–1650
https://doi.org/10.1007/s10494-025-00680-5

RESEARCH

Assessment of Approximate Soret Diffusion Models for Hydrogen and Ammonia Combustion

Thorsten Zirwes[1] · **Andreas Kronenburg**[1]

Received: 1 April 2025 / Accepted: 14 July 2025 / Published online: 24 July 2025

Abstract
Detailed modeling of combustion processes involving hydrogen poses challenges due to the high diffusivities of the light hydrogen molecule (H_2) and radical (H) compared to other species. Thermodiffusion, also known as the Soret effect, describes the diffusive flux of species induced by gradients of temperature. The Soret effect becomes important if the fuel species is much lighter (or heavier) than the mean molar mass of the mixture. While accurate models for Soret diffusion exist, e.g. the multicomponent diffusion model, they are usually computationally expensive. In this work, modeling strategies for approximating Soret diffusion available in popular software packages as well as additional models from the literature are assessed in terms of their accuracy. Four methods for computing reduced collision integrals are compared and three formulations for the thermodiffusion coefficients are investigated for hydrogen and ammonia combustion. All tested approaches for computing collision integrals are found to yield good results. The approximate Soret diffusion model by Chapman and Cowling has shown the best prediction accuracy for typical hydrogen flames and ammonia/hydrogen blends when compared to the multicomponent diffusion model. Results are also compared to the model by Hirschfelder and Warnatz, implemented in the popular software packages Chemkin and STAR-CD, and the model by Bartlett and coworkers, which is available in Ansys Fluent, using different benchmark cases. This work shall serve as a review of implementation details of common models as well as a guideline for accurate and efficient Soret diffusion modeling in future hydrogen and ammonia combustion simulations.

Keywords Soret effect · Thermodiffusion · Hydrogen · Ammonia · Laminar flames

✉ Thorsten Zirwes
thorsten.zirwes@irst.uni-stuttgart.de

Andreas Kronenburg
andreas.kronenburg@irst.uni-stuttgart.de

[1] Institute for Reactive Flows (IRST), University of Stuttgart, Pfaffenwaldring 31, 70569 Stuttgart, Germany

1 Introduction

Decreasing greenhouse gas emissions is a pressing issue of our time. Because of this, changes in the energy supply chain have to be implemented. One important building block in the near-future energy landscape is hydrogen because it can be produced from renewable sources and stored as a chemical energy carrier. As a carbon-free fuel, hydrogen can be burned without carbon dioxide emissions. To overcome difficulties associated with storage and transport of hydrogen, it can be converted to ammonia. The ammonia can then be burned directly, or together with hydrogen to increase flame stability.

However, hydrogen poses challenges to current combustion systems as well as modeling strategies. Hydrogen exhibits higher reactivity than typical hydrocarbon fuels (Lapenna et al. 2023) and faster diffusion velocities than other species in the gas mixture. For lean hydrogen flames, this can result in thermodiffusive instabilities that can significantly change the global propagation speed of laminar (Berger et al. 2023, 2022, 2019; Lulic et al. 2022; Zhang et al. 2022; Gaucherand et al. 2023) and turbulent flames (Dinesh et al. 2016; Rieth et al. 2022; Zirwes et al. 2022; Howarth et al. 2023) and lead to other phenomena like local flame quenching (Shi et al. 2023; Chen et al. 2021; Howarth and Aspden 2022), tip opening in Bunsen flames (Law et al. 1982; Zirwes et al. 2021) and the formation of cellular structures (Law et al. 2005; Hu et al. 2009; Patyal and Matalon 2018, 2022; Wen et al. 2021a, 2021b; Eckart et al. 2022). Detailed modeling of these phenomena requires the use of accurate diffusion models.

In the past decades, different approaches have been developed for calculating accurate diffusion fluxes. Apart from the usual mass diffusion due to concentration gradients, the Soret effect has to be considered as well for hydrogen flames. The Soret effect describes the diffusion of chemical species due to temperature gradients. Accurate Soret diffusion models are required to predict the correct flame speed of hydrogen flames, which has significant impact on design and safety decisions for burner development. It is also an important aspect in direct numerical simulations (DNS), which fully resolve the flame front to study more fundamental aspects of hydrogen flames. Recent DNS studies focused on thermodiffusive instabilities, which arise from the interplay of local flame speeds and flame stretch rates, in laminar configurations (Berger et al. 2019; Howarth et al. 2023; Aspden et al. 2011; Zirwes et al. 2024), as well as turbulence-flame interaction (Rieth et al. 2022, Gaucherand et al. 2024; Lee et al. 2022; Song et al. 2021), where turbulent flame speeds were found to significantly be determined by molecular diffusion of hydrogen (Lapenna et al. 2024). Likewise, the complex mass and Soret diffusion characteristics of hydrogen flames pose challenges for developing subgrid models (Lapenna et al. 2021; Aniello et al. 2022), which is why accurate flame databases from DNS must be provided to aid further model development.

Sutherland et al. (2005) and Grcar et al. (2009) showed the importance of Soret diffusion for hydrogen flames in terms of flame dynamics. Schlup and Blanquart (2018b) compared different modeling approaches for 1D, 2D and 3D applications. Howarth et al. (2024) found that the Chapman and Cowling (1970) model can be a good approximation for the more detailed multicomponent Soret model. Zirwes et al. (2024) showed that the presence of Soret diffusion changes the way thermodiffusive instabilities in hydrogen flames grow in 2D and 3D.

While accurate models for calculating Soret diffusion coefficients exist, like in the framework of the multicomponent diffusion model (Kee et al. 2005), these models are usually

computationally expensive. Therefore, simulations in 3D are commonly performed with simplified models, like the mixture-averaged diffusion model. However, the mixture-averaged model does not provide a description for Soret diffusion coefficients. Because of this, approximate models for calculating Soret diffusion models are usually employed when running 3D simulations.

The goal of this work is to assess different approximate Soret diffusion models that can be used together with the mixture-averaged diffusion model, and to provide guidelines for accurate hydrogen combustion simulations as well as hydrogen/ammonia blends, which have been gaining attention in the combustion community (Chai et al. 2021; Zirwes et al. 2023; Tamadonfar et al. 2024, 2025; Girhe et al. 2024). We focus on models that are available in popular simulation software, such as Chemkin, STAR-CD and Fluent, and discuss implementation details and review model variations from the literature. The scope of this work is limited to models that can be used together with the mixture-averaged diffusion model and that can be easily integrated into existing frameworks such as Chemkin or Cantera. Therefore, we do not consider iterative approaches (Córdoba and Arias-Zugasti 2022), approaches that require additional pre-processing steps (Hall and Pitz 2016), or mixed-method approaches (Xin et al. 2015). To the best knowledge of the authors, this is the first comprehensive study evaluating three different approximate Soret diffusion models, including several variations found in the literature, together with four collision integral modeling approaches, applied to hydrogen combustion and ammonia/hydrogen blends.

The paper is structured as follows: Sect. 2 introduces the fundamental description of detailed diffusion modeling and establishes a baseline configuration for hydrogen-air flames. Section 3 reviews different modeling approaches from the literature for approximate Soret diffusion models. In Sect. 4, a direct comparison of evaluation methods for collision integrals is provided, which is the basis for some of the approximate Soret diffusion models discussed next. Section 5 provides analysis of the accuracy of three popular Soret diffusion models, discussing further model variations and their limitations. The analysis is performed by directly evaluating Soret diffusion coefficients based on given canonical flame profiles. Section 6 continues this evaluation by comparing laminar flame speeds from different approximate Soret diffusion models with the multicomponent diffusion model under a wide range of operating conditions for hydrogen-air flames. Section 7 extends this assessment to ammonia/hydrogen blends by focusing on flame dynamics in counterflow twin flames. Results and recommendations are summarized in Sect. 8.

2 Diffusion Modeling

In this section, we will briefly outline the basic modeling strategies in the multicomponent and mixture-averaged diffusion models. Assuming ideal gases, negligible pressure gradients and no species-specific forces like magnetic forces for charged species, the total diffusive flux $\mathbf{j}_k$ of any species k can generally be expressed as

$$\mathbf{j}_k = \mathbf{j}_k^{\text{mass}} + \mathbf{j}_k^{\text{Soret}} + \mathbf{j}_k^{\text{corr}}, \tag{1}$$

where $\mathbf{j}_k^{\text{mass}}$ is the diffusive flux of species k due to gradients of the species mole or mass fractions (see below) and $\mathbf{j}_k^{\text{Soret}}$ is the diffusive flux of species k due to the gradient of tem-

perature, i.e. the Soret effect. A correction flux $\mathbf{j}_k^{\text{corr}}$ is introduced to assure that the sum of all fluxes equals zero

$$\sum_k \mathbf{j}_k \stackrel{!}{=} 0, \tag{2}$$

so that

$$\mathbf{j}_k^{\text{corr}} := -Y_k \sum_i \left(\mathbf{j}_i^{\text{mass}} + \mathbf{j}_i^{\text{Soret}}\right), \tag{3}$$

where Y_k is the mass fraction of species k and the index i iterates over all species.

In most established combustion codes, like Cantera and Chemkin, the most accurate way of calculating diffusive fluxes is the multicomponent diffusion model. By inverting the Maxwell–Stefan relations, the following formulation can be derived (Kee et al. 2005)

$$\mathbf{j}_{\text{multi},k}^{\text{mass}} = \rho Y_k \frac{1}{X_k \bar{M}} \sum_{i \neq k} M_i D_{k,i} \nabla X_i, \tag{4}$$

where ρ is the mixture density, X_k the mole fraction of species k, $\bar{M}$ the mean molar mass of the mixture and M_i the molecular mass of species i. $D_{k,i}$ is the multicomponent diffusion coefficient for the species pair k and i. The Soret diffusion flux is expressed as

$$\mathbf{j}_k^{\text{Soret}} = -D_k^{\text{Soret}} \frac{1}{T} \nabla T, \tag{5}$$

where T is the temperature and D_k^{Soret} is the Soret or thermodiffusion coefficient of species k. Using the multicomponent diffusion models, the following relations are guaranteed

$$\sum_k \sum_i M_k M_i D_{k,i} \nabla X_i = 0 \tag{6}$$

$$\sum_k D_k^{\text{Soret}} = 0 \tag{7}$$

so that

$$\sum_k \mathbf{j}_{\text{multi},k}^{\text{mass}} = 0, \qquad \sum_k \mathbf{j}_{\text{multi},k}^{\text{Soret}} = 0, \qquad \mathbf{j}_{\text{multi},k}^{\text{corr}} = 0. \tag{8}$$

While the multicomponent diffusion model is the most accurate of the commonly employed diffusion models, it is computationally very expensive. It requires a matrix inversion to obtain the diffusion coefficients $D_{k,i}$. In contrast to the mixture-averaged diffusion model, which is discussed next, the multicomponent diffusion model provides the Soret diffusion coefficients D_k^{Soret} as part of the matrix inversion, the details of which can be found elsewhere (Kee et al. 2005).

Due to the computational cost involved with the multicomponent diffusion model, most detailed simulations performed in 3D are conducted using the less expensive mixture-averaged diffusion model. Assuming that from the point of view of species k all other species diffuse with a mixture-averaged diffusion velocity, different Fick-like mass diffusion formulations can be derived. Usually, they are formulated in terms of mole fraction gradients

$$\mathbf{j}^{\text{mass}}_{\text{mix,mole},k} = -\rho \frac{M_k}{\bar{M}} D^{\text{mole}}_{\text{mix},k} \nabla X_k \tag{9}$$

or in terms of mass fraction gradients

$$\mathbf{j}^{\text{mass}}_{\text{mix,mass},k} = -\rho D^{\text{mass}}_{\text{mix},k} \nabla Y_k. \tag{10}$$

Note that Eqs. (9) and (10) are derived with a similar set of assumptions, but both formulations are not equal. The Fick diffusion coefficients appearing in the two formulations are (Kee et al. 2005)

$$D^{\text{mole}}_{\text{mix},k} = \frac{1 - Y_k}{\sum_{i \neq k} \frac{X_i}{\mathcal{D}_{i,k}}}, \qquad D^{\text{mass}}_{\text{mix},k} = \left(\sum_{i \neq k} \frac{X_i}{\mathcal{D}_{k,i}} + \frac{X_k}{1 - Y_k} \sum_{i \neq k} \frac{Y_i}{\mathcal{D}_{k,i}} \right)^{-1}, \tag{11}$$

where $\mathcal{D}_{k,i}$ are the binary Maxwell–Stefan diffusion coefficients (not to be confused with the multicomponent diffusion coefficients $D_{k,i}$ from Eq. (4)) usually computed from the Chapman–Enskog solution of the Boltzmann equation. Due to the assumptions underlying the mixture-averaged diffusion model, its application is generally justified in dilute mixtures, e.g. combustion in air where N_2 makes up the majority of the gas mixture. Note that for the mixture-averaged diffusion model, in contrast to the multicomponent model, the sum of diffusive mass fluxes is not guaranteed to be zero so that the correction flux must be included. While the mixture-averaged diffusion models provide an efficient and accurate way of modeling diffusive mass fluxes for many applications, it does not provide a way to compute Soret diffusion coefficients. Therefore, approximate Soret diffusion models must be employed.

In the remainder of this work, detailed Soret diffusion coefficients from the multicomponent diffusion model are compared with coefficients from approximate Soret diffusion models for use together with the mixture-averaged diffusion model. To provide a good baseline for the following discussion, Fig. 1 compares the laminar flame speed s_L^0 obtained with Cantera (Goodwin et al. 2024) for hydrogen-air flames at atmospheric conditions and different equivalence ratios ϕ, without taking Soret diffusion into account. Shown are results from the multicomponent diffusion model and the two formulations of the mixture-averaged diffusion model, based on the reaction mechanism by Li et al. (2004). Since the agreement of flame speeds without Soret diffusion is best between the multicomponent model (black solid line) and the mixture-averaged model based on mass fraction gradients (red dotted line), all following calculations will be done with the mixture-averaged diffusion model based on Eq. (10).

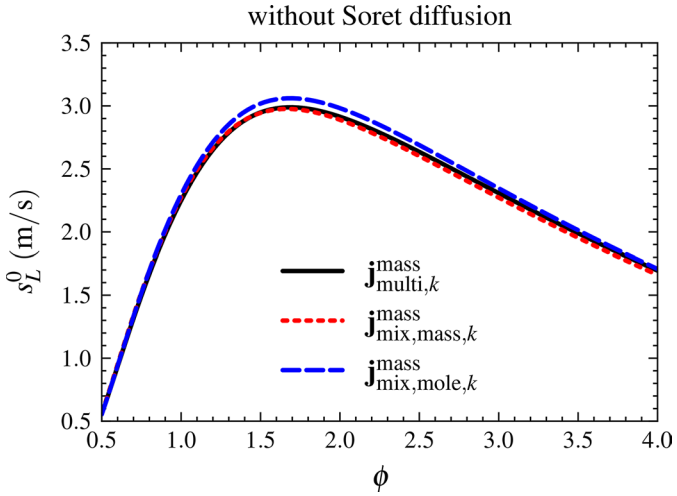

Fig. 1 Laminar flame speed for hydrogen-air flames at $T_0 = 300\,\text{K}$ and $p = 1\,\text{atm}$ without Soret diffusion for different equivalence ratios ϕ. Air is assumed as $X_{\text{O}_2} = 0.21$, $X_{\text{N}_2} = 0.79$

3 Approximate Soret Diffusion Models

Different approximate Soret models have been devised in the past for computing the Soret diffusion coefficients D_k^{Soret}. Here, we will focus on three of the most popular models. The first model is the one by Bartlett et al. (1968). This model is available as part of, e.g., the Ansys Fluent simulation software. In this model, the Soret diffusion coefficient is computed (here rewritten from the original cgs definition (Bartlett et al. 1968; Kuo and Acharya 2012) in terms of SI units) as (ANSYS 2009)

$$D^{\text{Soret}}_{\text{Bartlett},k} \approx -2.59 \times 10^{-7} \frac{\text{kg}}{\text{m s}} \left(\frac{T}{\text{K}}\right)^{0.659} \left(\frac{M_k^{0.511} X_k}{\sum_i M_i^{0.511} X_i} - Y_k\right) \frac{\sum_i \left(\frac{M_i}{\frac{\text{g}}{\text{mol}}}\right)^{0.511} X_i}{\sum_i \left(\frac{M_i}{\frac{\text{g}}{\text{mol}}}\right)^{0.489} X_i}. \quad (12)$$

Note that the molar masses M_i have to be provided in g/mol. It is also interesting to note that this formulation guarantees $\sum_k D^{\text{Soret}}_{\text{Bartlett},k} = 0$.

The second type of models expresses the Soret diffusion coefficient using the thermal diffusion ratio Θ_k and the mass diffusion coefficient $D^{\text{mole}}_{\text{mix},k}$ from Eq. (9) as

$$D_k^{\text{Soret}} \approx c_k\, f_k \rho \frac{M_k}{\bar{M}} D^{\text{mole}}_{\text{mix},k} \Theta_k, \quad (13)$$

where f_k is a model constant, usually set to $f_k = \frac{1}{2}$ and c_k is a model constant usually set to unity. See below for further discussion.

In the model by Chapman and Cowling (C& C) (1970), which was recently further assessed by Schlup and Blanquart (2018b) and earlier by Paul and Warnatz (1998), the thermal diffusion ratio is given by

$$\Theta_k^{\mathrm{C\&C}} = \frac{15}{2}\frac{\bar{M}^2}{\rho}\sum_i \left(\frac{1.2C^{\star}_{k,i}-1}{\mathcal{D}_{k,i}}\right)\left(\frac{Y_k\frac{\mu_i}{M_i}a_i - Y_i\frac{\mu_k}{M_k}a_k}{M_k+M_i}\right). \tag{14}$$

Note that in some works, the factor $\frac{15}{2}$ in Eq. (14) is summarized as $c_k\, f_k \frac{15}{2} = \frac{15}{4}$. While using $\frac{15}{4}$ has physical meaning in the derivation of the model, we choose $\frac{15}{2}$ here to provide a unified formulation between the different models. μ_i are the pure-species viscosities, $C^{\star}_{k,i}$ is the ratio of reduced collision integrals, discussed in the next section, and a_k is given by

$$a_k = \left(1 + \frac{1.065}{2\sqrt{2}X_k}\sum_{i\neq k} X_i\Phi_{k,i}\right)^{-1}, \tag{15}$$

where $\Phi_{k,i}$ is the mixing operator from the Wilke mixing formula (Poling et al. 2001). Note that, depending on the definition, the factor $1/\sqrt{2}$ can also be defined as part of $\Phi_{k,i}$.

The model by Warnatz (1982), based on previous work by Hirschfelder (1964) (H& W), which is found for example in the popular simulation tools Chemkin and STAR-CD, expresses Θ_k as

$$\Theta_k^{\mathrm{H\&W}} = \sum_i R_{k,i}\frac{M_k - M_i}{M_k + M_i}X_iX_k. \tag{16}$$

Here, $R_{k,i}$, the thermal diffusion factor, is only a function of the reduced temperature, discussed in the next section. The H& W model is derived for light species, which are most affected by Soret diffusion. Therefore, it is common to use this model only for the light species with $M_k < 5\,\mathrm{kg/kmol}$, which in most combustion cases will be H, H_2 and He, and to set the Soret diffusion coefficient to zero for all other species.

Different authors and implementations prefer different values for the model constants. As indicated above, $f_k = \frac{1}{2}$ and $c_k = 1$ are the most common choices. However, different conventions exist. Other modifications of these constants found in the literature are (Siemens 2017),

$$f_k = \frac{1}{2}, \qquad f_k = \begin{cases} 0.5, & \text{if } X_k \leq 0.5 \\ 0.9, & \text{if } X_k > 0.5 \end{cases}, \qquad f_k = 1, \tag{17}$$

and (Sanders 1994)

$$c_k = 1, \qquad c_k = \frac{1-Y_k}{1-X_k} \text{ if } (1-X_k) > 10^{-10}. \tag{18}$$

For all investigated cases in this work, among the variations from Eq. (17), $f_k = \frac{1}{2}$ was found to have the best prediction accuracy. Therefore, for the remainder of this work, $f_k = \frac{1}{2}$ will be assumed. It should be noted that accuracy can be improved by tuning this value for specific applications (Howarth et al. 2024; Schlup and Blanquart 2018a), which is not in the scope of this work.

Another consideration is the normalization of Soret diffusion coefficients. In the multicomponent and Bartlett et al. (1968) models, it is guaranteed that $\sum_k D_k^{\mathrm{Soret}} = 0$, so that

no need for a correction flux $\mathbf{j}_k^{\mathrm{corr}}$ arises from Soret diffusion. This guarantee is not given by the C& C and H& W models. One way of normalization is to define the final Soret diffusion coefficients as

$$\hat{D}_k^{\mathrm{Soret}} = D_k^{\mathrm{Soret}} - Y_k \sum_i D_i^{\mathrm{Soret}}, \tag{19}$$

which guarantees that $\sum_k \mathbf{j}_k^{\mathrm{Soret}} = 0$. Note, however, that this method can only be used if D_k^{Soret} are computed for all species. If only light species are considered, the correction must be done through $\mathbf{j}_k^{\mathrm{corr}}$ according to Eq. (3). From a practical point of view, including all species and using Eq. (19) to normalize the Soret diffusion coefficients is more convenient since Soret diffusion fluxes can then be easily computed as a postprocessing step from $\hat{D}_k^{\mathrm{Soret}}$ and the temperature field without the need of evaluating $\mathbf{j}_k^{\mathrm{corr}}$. As shown later, the choice if Soret diffusion coefficients are calculated for only the light species or all species has shown negligible influence for the overall flame properties.

4 Collision Integrals

In the H& W and C& C models, some quantities appear that are computed from collision integrals. In this section, we compare different common approaches from popular software packages. These quantities are typically provided as a function of the reduced temperature

$$T_{k,i}^{\star} = \frac{k_B T}{\epsilon_{k,i}}, \tag{20}$$

where k_B is Boltzmann's constant and

$$\epsilon_{k,i} = \sqrt{\epsilon_k \epsilon_i}, \tag{21}$$

where ϵ_k is the Lennard-Jones potential well depth of species k. In this formulation, $T_{k,i}^{\star} = T_{i,k}^{\star}$. Other software packages, like Cantera, include a correction for the polarity of the species (Hirschfelder et al. 1964)

$$\epsilon_{k,i} = \sqrt{\epsilon_k \epsilon_i} \xi_{k,i}^2, \tag{22}$$

so that $T_{k,i}^{\star} \neq T_{i,k}^{\star}$. We found negligible influence of the inclusion of the polar correction on Soret diffusion coefficients in hydrogen combustion systems.

The parameter $R_{k,i}$ from Eq. (16) can be approximated by a piecewise linear fit (Chapman and Cowling 1970; Sanders 1994):

$$R_{k,i} = \begin{cases} 0, & \text{if } T^\star_{k,i} \le 1 \\ 0.015 + 0.3000(T^\star_{k,i} - 1.0), & \text{if } 1.0 < T^\star_{k,i} \le 1.7 \\ 0.225 + 0.1880(T^\star_{k,i} - 1.7), & \text{if } 1.7 < T^\star_{k,i} \le 2.5 \\ 0.375 + 0.0970(T^\star_{k,i} - 2.5), & \text{if } 2.5 < T^\star_{k,i} \le 4.0 \\ 0.520 + 0.0264(T^\star_{k,i} - 4.0), & \text{if } 4.0 < T^\star_{k,i} \le 6.5 \\ 0.600, & \text{if } T^\star_{k,i} > 6.5 \end{cases} \tag{23}$$

Another commonly used expression is (Hirschfelder et al. 1964)

$$R_{k,i} = \frac{15}{2} \frac{(2A^\star_{k,i} + 5)(6C^\star_{k,i} - 5)}{A^\star_{k,i}(16A^\star_{k,i} - 12B^\star_{k,i} + 55)}, \tag{24}$$

where $C^\star_{k,i}$ is the same quantity as the one appearing in Eq. (14). In programs like Chemkin, $A^\star_{k,i}$, $B^\star_{k,i}$ and $C^\star_{k,i}$ are available as fits of $T^\star_{k,i}$. In Cantera, $A^\star_{k,i}$, $B^\star_{k,i}$ and $C^\star_{k,i}$ are computed from tabulated values as a function of $T^\star_{k,i}$ as well as the dipole moment $\delta_{k,i}$ of the species pair.

In STAR-CD and other programs, the collision integral ratios are approximated using the formulation

$$A^\star_{k,i} = \frac{\Omega^{(2,2)^\star}_{k,i}}{\Omega^{(1,1)^\star}_{k,i}}, \qquad B^\star_{k,i} = \frac{5\Omega^{(1,2)^\star}_{k,i} - 4\Omega^{(1,3)^\star}_{k,i}}{\Omega^{(1,1)^\star}_{k,i}}, \qquad C^\star_{k,i} = \frac{\Omega^{(1,2)^\star}_{k,i}}{\Omega^{(1,1)^\star}_{k,i}}, \tag{25}$$

and the reduced collision integrals are given by Neufeld et al. (1972)

$$\begin{aligned} \Omega^{(1,1)^\star}_{k,i} = {} & 1.06036 {T^\star_{k,i}}^{-0.15610} + 0.19300 e^{-0.47635 T^\star_{k,i}} \\ & + 1.03587 e^{-1.52996 T^\star_{k,i}} + 1.76474 e^{-3.89411 T^\star_{k,i}} \end{aligned} \tag{26}$$

$$\begin{aligned} \Omega^{(1,2)^\star}_{k,i} = {} & 1.00220 {T^\star_{k,i}}^{-0.15530} + 0.16105 e^{-0.72751 T^\star_{k,i}} \\ & + 0.86125 e^{-2.06848 T^\star_{k,i}} + 1.95162 e^{-4.84492 T^\star_{k,i}} \end{aligned} \tag{27}$$

$$\begin{aligned} \Omega^{(2,2)^\star}_{k,i} = {} & 1.16145 {T^\star_{k,i}}^{-0.14874} + 0.52487 e^{-0.77320 T^\star} + 2.16178 e^{-2.43787 T^\star_{k,i}} \\ & -0.0006435 {T^\star_{k,i}}^{0.14874} \sin\left(18.0323 {T^\star_{k,i}}^{-0.76830} - 7.27371\right) \end{aligned} \tag{28}$$

$$\begin{aligned} \Omega^{(1,3)^\star}_{k,i} = {} & 0.96573 {T^\star_{k,i}}^{-0.15611} + 0.44067 e^{-1.52420 T^\star_{k,i}} + 2.38981 e^{-5.08063 T^\star_{k,i}} \\ & -0.0005373 {T^\star_{k,i}}^{0.15611} \sin\left(19.2866 {T^\star_{k,i}}^{-1.30775} - 6.58711\right) \end{aligned} \tag{29}$$

where the last terms in Eqs. (32) and (31) containing the sine function are often neglected. Note that the relations from Eq. (25) depend on the definition of the collisions integrals and other definitions exist in the literature (Dixon-Lewis 1968).

Figure 2 shows the values of $R_{k,i}$ and $C^\star_{k,i}$ based on the different approximations described above. Note that for Cantera, the dipole moment was set to zero and the polar correction was switched off so that $R_{k,i}$ and $C^\star_{k,i}$ are purely functions of $T^\star_{k,i}$ in all cases.

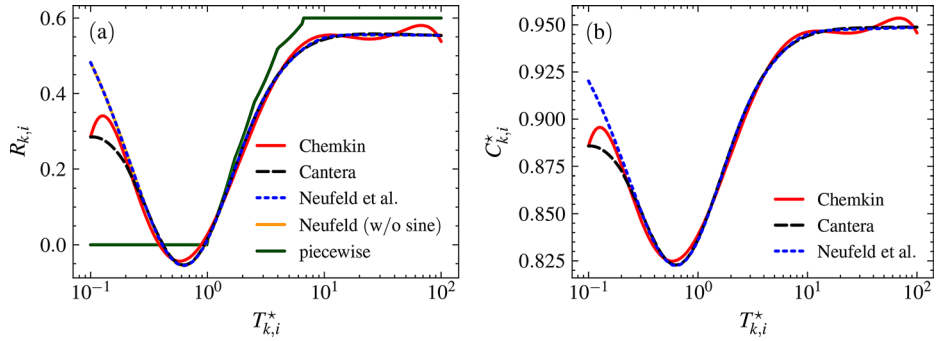

Fig. 2 (**a**) $R_{k,i}$ and (**b**) $C^\star_{k,i}$ computed with different approximations from popular software packages as a function of $T^\star_{k,i}$

In the figure, we refer to the model according to authors from the publications cited above or the software package where they are commonly found. The inclusion of the additional sine terms from Eqs. (32) and (31) can be neglected (compare the orange solid and blue dotted line in Fig. 2a). Some minor differences between the models are visible for $T^\star_{k,i} < 0.5$, which is often not relevant for practical combustion applications. Similarly, for large values of $T^\star_{k,i} > 10$, minor differences appear. The piece-wise approximation shows the largest deviation for $R_{k,i}$ from the other models for small and large values of $T_{k,i}$. However, using all the different models, negligible differences for the Soret diffusion coefficients were found. Because of this, we will evaluate all collision integral-related quantities with the methods provided by Cantera, including dipole moments and polar corrections, in the remainder of this work.

5 Direct Comparison of Soret Diffusion Coefficients

The goal of this work is to assess approximate Soret diffusion models for use together with the mixture-averaged diffusion model. In this section, the performance of the different models is evaluated by comparing the Soret diffusion coefficients with those calculated from the multicomponent diffusion model. In order to avoid any differences stemming from the general model differences between the multicomponent and mixture-averaged models and to focus solely on the prediction of Soret diffusion coefficients, we first perform perform 1D freely-propagating hydrogen-air flame simulations with Cantera using the multicomponent diffusion model. In this way, we can evaluate Soret diffusion coefficients as a second post-processing step with all different Soret diffusion models. This ensures that observed differences arise only from the Soret diffusion models and not the flame simulation itself. In this section, $c_k = 1$ in Eq. (13) is assumed for all cases.

Figure 3 shows results from a 1D freely-propagating hydrogen-air flame at atmospheric conditions computed with Cantera using the multicomponent diffusion model with Soret diffusion. The flame is computed for an equivalence ratio $\phi = 0.4$ (left column), which is often used as a reference composition when discussing thermodiffusive instabilities (Berger et al. 2019), and $\phi = 1$ (right column). The Soret diffusion coefficients from the multicomponent model, which serve as the reference values, are given as black solid lines through the

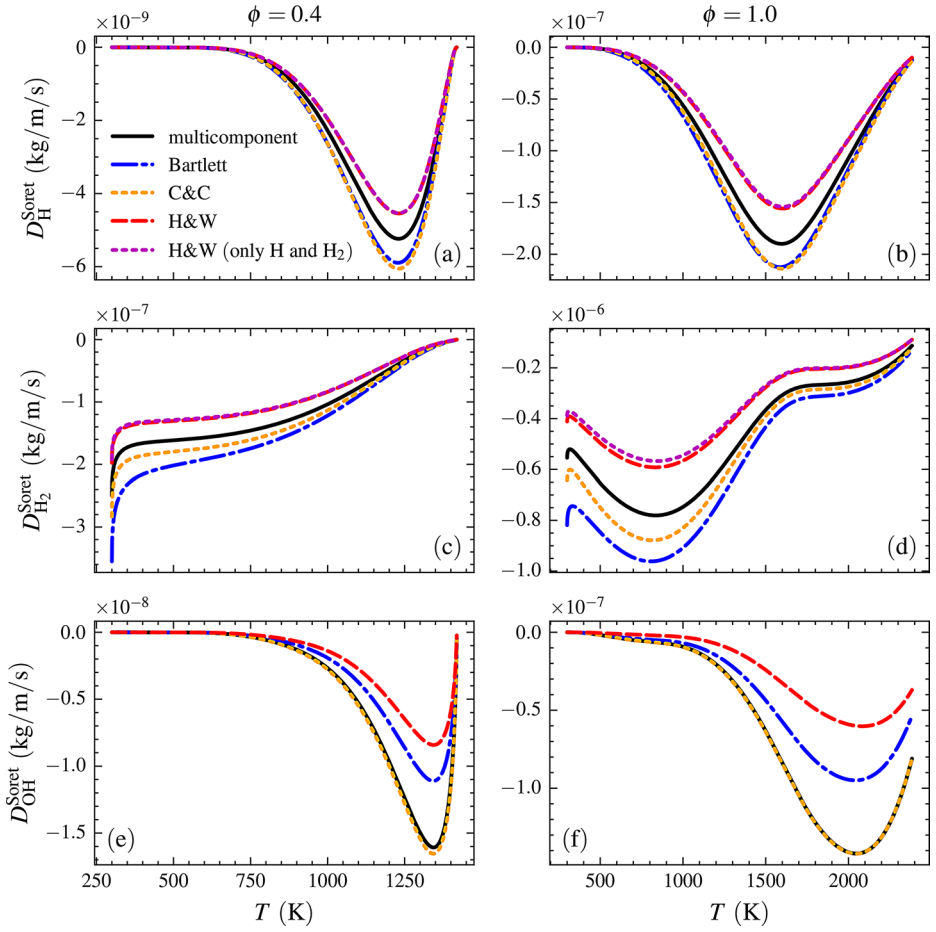

Fig. 3 Soret diffusion coefficients along a 1D freely propagating hydrogen-air flame at atmospheric conditions and $\phi = 0.4$ and $\phi = 1$ Coefficients for H (top row), H_2 (middle row) and OH (bottom row) are evaluated as a post-processing step from the multicomponent flame solution

flame. Soret coefficients from the approximate models are computed as a post-processing step based on the mixture composition and temperature at each point of that flame. Soret coefficients are plotted over the temperature profile of the flame (unburnt gas on the left, burnt gas on the right). Shown are Soret diffusion coefficients for H (top row), H_2 (middle row) and OH (bottom row).

All approximate models capture the general trend of the values from the multicomponent model. Accurate predictions for H and H_2 are most important to correctly incorporate the effect of Soret diffusion on overall flame dynamics. While all models have some deviations for these two species, the C& C model has the closest agreement for these two species at stoichiometric conditions and performs very similarly to the model by Bartlett. For heavier species like OH, shown in the bottom row, the C& C model performs best. Note however that the H& W model is derived specifically for light species, and that heavy species do not have a large influence in terms of the Soret effect for hydrogen combustion. For the H& W

model, choosing to compute Soret diffusion coefficients only for H and H_2 or for all species only results in minor differences, as best seen in Fig. 3d, comparing the red dashed and magenta dotted lines.

In order to provide a more quantitative comparison, Table 1 shows the normalized error of the Soret diffusion coefficient calculated as

$$\varepsilon_k = \frac{\sqrt{\frac{1}{N}\sum_{n=1}^{N}\left(D^{\text{Soret}}_{\text{M},k,n} - D^{\text{Soret}}_{\text{Multi},k,n}\right)^2}}{\max\left|D^{\text{Soret}}_{\text{Multi},k}\right|}, \tag{30}$$

where ε_k is the normalized error compared to the multicomponent model ($D^{\text{Soret}}_{\text{Multi},k,n}$ denotes the multicomponent Soret diffusion model for species k at grid point n) for the approximate Soret model M and species k over all N grid points of the freely propagating flame at the given equivalence ratio. The grid points are taken directly from the Cantera simulation. Due to the adaptive mesh refinement, the point distribution depends on the gradients and curvatures of all species profiles, keeping biases towards all species low while calculating the averaged error terms. A lean ($\phi = 0.4$), stoichiometric ($\phi = 1$) and rich flame ($\phi = 4$) are considered. All models show good accuracy for H and H_2 at all conditions. On average, the C& C model performs best. Interestingly, all models are able to predict Soret diffusion coefficients for other species well for lean to stoichiometric conditions, while for rich flames, the prediction accuracy decreases. Predictions of H and H_2, which are the most important species for Soret diffusion, are best predicted at rich conditions by the C& C model among the three models. The same trends were found using a different hydrogen reaction mechanism by Burke et al. (2012) and Boivin (2011) (see supplementary material B). Soret diffusion coefficients of water at rich conditions show the largest deviation to the multicomponent results. Generally, the assumptions used in the model derivations may not hold for nonlinear and heavy species, which might explain this deviation. Nonetheless, the impact of water Soret diffusion coefficients on overall flame dynamics is generally low.

Although not the focus of this work, Soret diffusion also becomes relevant if the fuel species is significantly heavier than the mean molar mass of the mixture. The supplementary material A adds an additional evaluation of Soret diffusion coefficient for kerosene, which is well predicted by the C& C model, while the H& W model, which is derived assuming only light species, cannot be used in this case.

Table 1 Normalized error of the Soret diffusion coefficient prediction from three approximate models for different species, ε_k, in a lean, stoichiometric and rich hydrogen-air flame at atmospheric condition. Green color shows low errors, red shows large errors

	Bartlett et al.			H&W			C&C		
Species	$\phi = 0.4$	$\phi = 1$	$\phi = 4$	$\phi = 0.4$	$\phi = 1$	$\phi = 4$	$\phi = 0.4$	$\phi = 1$	$\phi = 4$
H	0.05	0.06	0.13	0.06	0.09	0.19	0.07	0.06	0.04
H_2	0.18	0.22	0.28	0.11	0.17	0.25	0.07	0.09	0.10
H_2O_2	0.04	0.10	0.24	0.20	0.13	0.03	0.02	0.06	0.33
HO_2	0.06	0.06	0.23	0.25	0.18	0.04	0.09	0.02	0.34
OH	0.13	0.14	0.34	0.21	0.25	2.21	0.01	0.00	1.10
O	0.14	0.16	0.13	0.21	0.28	1.00	0.02	0.04	0.49
O_2	0.11	0.19	0.37	0.32	0.21	0.08	0.06	0.06	0.41
H_2O	0.08	0.09	1.29	0.27	0.24	5.65	0.10	0.06	5.63
N_2	0.12	0.09	0.21	0.28	0.25	0.36	0.13	0.05	0.07

6 Predicted Flame Speeds

In this section, we compare the performance of the different approximate models by computing laminar flame speeds. Note that in this case, the laminar flame speed is computed by running a 1D flame simulation with the mixture-averaged diffusion model together with one of the approximate Soret diffusion models, and comparing the results to the laminar flame speed from a 1D simulation with the multicomponent model. Again, we consider hydrogen-air flames at different equivalence ratios as well as pressures and pre-heating conditions.

In Fig. 4, laminar flame speeds at atmospheric conditions are shown, using either the multicomponent model, or the mixture-averaged model with one of the approximate Soret diffusion models. Compared with Fig. 1, the range of equivalence ratios is limited to $\phi = [1, 2.5]$, in order to show the differences between the models more clearly. Note that these conditions are chosen, because lean flames show only a week influence of the Soret effect on laminar, unstretched flame speeds. The gray line with the highest flame speed is from a simulation using the multicomponent diffusion model without Soret diffusion. Thus, the gray line from Fig. 4 is the same as the black line in Fig. 1, serving as a visual indication how strongly the Soret diffusion affects flame speeds.

The black solid line in Fig. 4 shows the reference results from the multicomponent model with Soret diffusion enabled. The C& C model shows the closet agreement with the reference, followed by the Bartlett model. Using $c_k = \frac{1-Y_k}{1-X_k}$ (see Eq. (18)) results in minor improvements for the C& C model and minor deviations for the H& W model (not shown here). As shown in supplementary material B, these trends are also independent of the choice of reaction mechanism (tested with the mechanisms by Burke et al. (2012) and Boivin (2011)). A comparison with measurements is provided in supplementary material C.

To make this comparison more general, Fig. 5a shows the laminar flames speed at preheated conditions ($T_0 = 500\,\mathrm{K}$) and Fig. 5b at elevated pressure ($p = 5\,\mathrm{atm}$). For the preheated condition, the C& C model again shows the best performance, but the relative

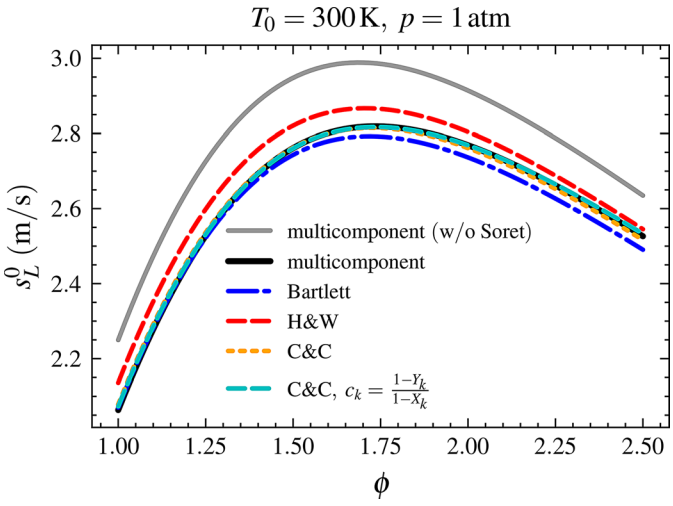

Fig. 4 Laminar flame speed s_L^0 for hydrogen-air flames at atmospheric conditions for different equivalence ratios and diffusion models

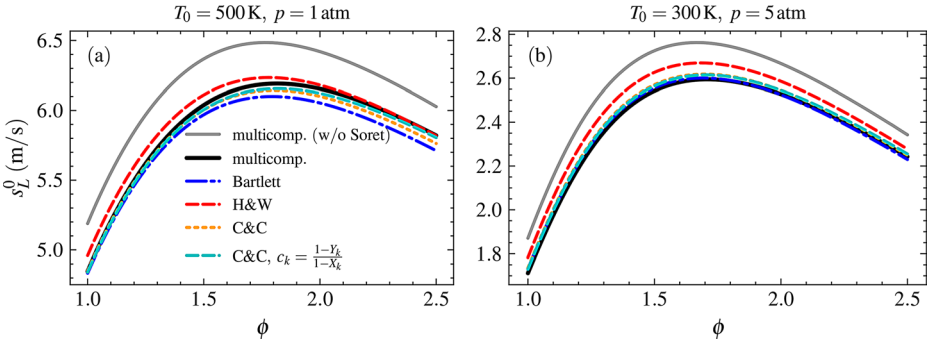

Fig. 5 Laminar flame speed s_L^0 for hydrogen-air flames at preheated (**a**) and elevated pressure (**b**) conditions for different equivalence ratios and diffusion models

performance of the H& W model is improved. At the elevated pressure, the model by Bartlett shows the best agreement, closely followed by the C& C model.

7 Ammonia/Hydrogen Blends

The last part of this study investigates the accuracy of the discussed approximate Soret diffusion models for ammonia/hydrogen blends. In the following, the reaction mechanism by Stagni et al. (2023) with 29 species and 203 reactions is chosen, because it is one of the best-performing mechanisms currently available for ammonia and ammonia/hydrogen blends, together with its predecessor version (Alnasif et al. 2023). For the study, we chose the ammonia/hydrogen blend of 60 vol-% NH_3 and 40 vol-% H_2, which is a commonly used blending ratio because of the similar flame speed characteristics as conventional methane-air flames.

In contrast to pure hydrogen flames, hydrogen/ammonia blends do not exhibit the same sensitivity of laminar flame speed to Soret diffusion. Figure 6 shows the flame speed as a function of equivalence ratio ϕ of the aforementioned ammonia/hydrogen blend at atmospheric conditions. Included are results from the multicomponent (gray line) and mixture-averaged model (cyan dashed line) without Soret diffusion, as well as the multicomponent model with Soret diffusion (black line) and the previously discussed approximate Soret diffusion models. Note that we activate Soret diffusion only for the light species (H and H_2) for the H& W model, as it is usually done in the literature and leads to negligible deviations as shown before, to simplify the discussion.

Instead of looking at the unstretched laminar flame speed, we choose a more challenging configuration where Soret diffusion exhibits a higher impact to evaluate the accuracy of the approximate Soret diffusion models. In the following, we look at the flame dynamics as a function of flame stretch in a premixed counterflow twin flame. Two opposing nozzles, both supplying the unburnt hydrogen/ammonia-air mixture at a given equivalence ratio at atmospheric conditions and the same velocity u, are placed $L = 2\,\mathrm{cm}$ apart. By increasing the speed of the nozzles u, the global flame stretch rate a_{global} is increased, which is defined here as

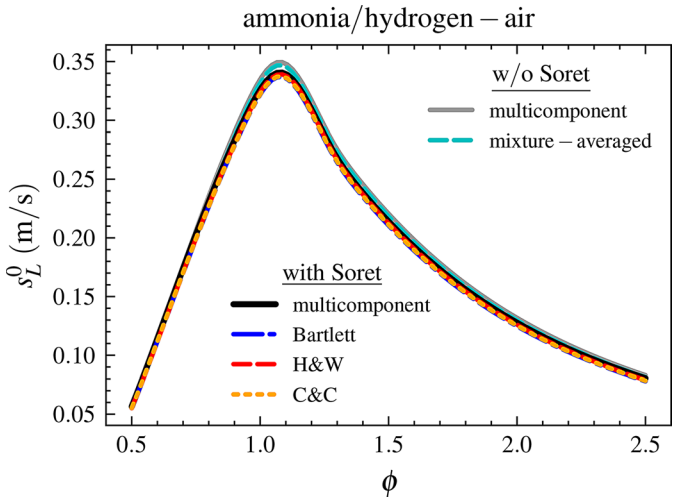

Fig. 6 Laminar flame speed s_L^0 for ammonia-air flames (60/40 by volume) at different equivalence ratios at atmospheric conditions (300 K and 1 atm)

$$a_{\text{global}} = \frac{2|u|}{L}. \tag{31}$$

For large enough a_{global}, the stretch rate increases up to the extinction strain and the flame quenches. For the purpose of evaluating the Soret diffusion models, we only consider rich ammonia/hydrogen mixtures. These exhibit a positive Markstein number, meaning that the decrease of flame speed with increasing flame stretch is primarily caused by the flame's sensitivity to flame stretch due to thermodiffusive effects. For lean mixtures, flame speeds increase with flame stretch and the quenching is instead primarily an effect of the flow residence times becoming too small. Figure 7 shows the maximum temperature (top) and consumption speed s_c in the counterflow twin flame configuration of the 60/40 ammonia/hydrogen blend at $\phi = 1.5$ (left) and $\phi = 2$ (right) as a function of global stretch rate for the different Soret models. The reference values are the results from the multicomponent model (thick black line). The consumption speed was evaluated from

$$s_c = \frac{1}{\rho_0(Y_{\text{O}_2,\text{eq}} - Y_{\text{O}_2,0})} \int \dot{\omega}_{\text{O}_2}\, \text{d}x, \tag{32}$$

where the subscript "0" denotes the unburnt condition, "eq" the value at chemical equilibrium and $\dot{\omega}_{\text{O}_2}$ is the reaction rate of O_2.

The trends from Fig. 7 confirm the same observations from the pure hydrogen flames: the closest agreement with the multicomponent model is provided by the $C\&C$ model. The H&W model tends to overpredict peak temperatures and consumption speeds, while the Bartlett model shows slight underpredictions. Because ammonia/hydrogen counterflow flames are sensitive to the choice of reaction mechanism (Girhe et al. 2024), the simulations discussed above are repeated for the KAUST mechanism (Zhang et al. 2021) and the mechanism by Konnov (2023) (see supplementary material D). While the KAUST mechanism yields

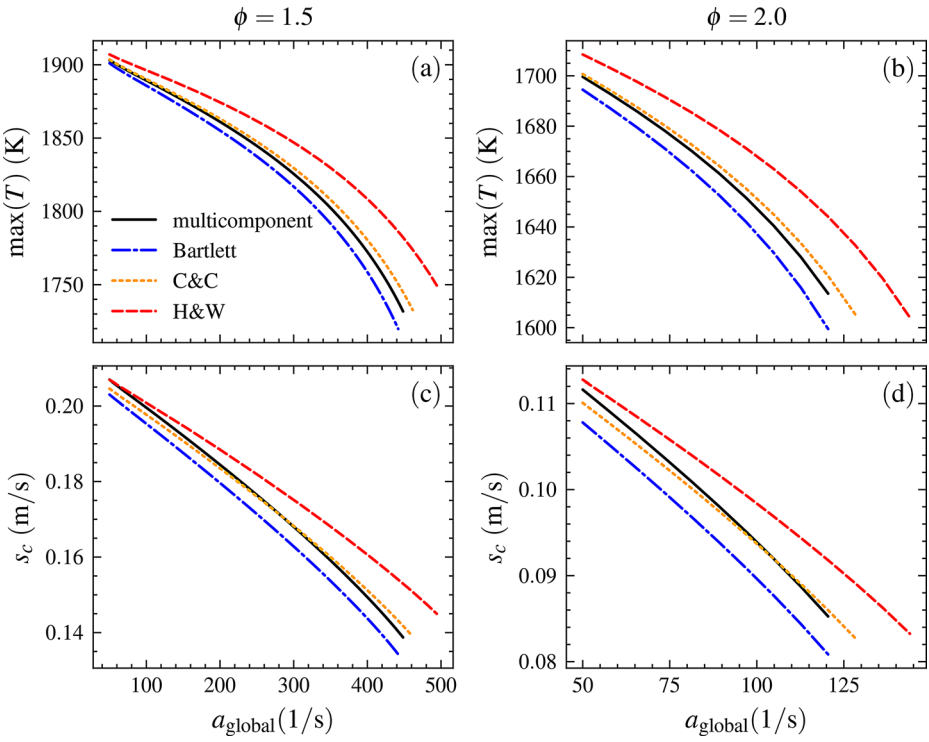

Fig. 7 Maximum temperature (top) and consumption speed (bottom) of rich ammonia/hydrogen flames (60/40 blend) plotted as a function of flame stretch until extinction for two equivalence ratios (left and right)

results similar to the one by Stagni et al., flame dynamics differ when using the mechanism by Konnov. Nonetheless, the same trends in terms of Soret model accuracy hold for these two mechanisms as well. While this work focuses on premixed combustion, where Soret diffusion is expected to play an important role, supplementary material E also includes an example of a non-premixed counterflow flame.

8 Conclusions

In this work, we have reviewed different approximate Soret diffusion models for use with the mixture-averaged diffusion model, and provided an overview of implementation details. In particular, we looked at the model by Bartlett and coworkers (Bartlett et al. 1968), which is found in Ansys Fluent, the model by Warnatz (1982) and Hirschfelder et al. (1964), commonly used in Chemkin and STAR-CD, and the Chapman and Cowling (1970) model. The focus of this work lies on the models' accuracy for hydrogen-air and ammonia/hydrogen-air flames. Model accuracy was assessed by comparing with results from the computationally expensive multicomponent diffusion model. All investigated models are able to predict the effect of Soret diffusion qualitatively. All models perform best in the lean to stoichiometric range for freely propagating flames. The model by Chapman and Cowling has shown the best results over a wide range of conditions, and can also be used for flames with heavy

fuels. At elevated pressure conditions, the Bartlett model performs also well. In terms of model constants, $f_k = \frac{1}{2}$ and $c_k = 1$ are the recommended values, while $c_k = \frac{1-Y_k}{1-X_k}$ can slightly improve the prediction quality of the Chapman and Cowling model in some cases. For ammonia/hydrogen blended flames, the C& C models shows the best performance, providing accurate predictions of flame speeds and peak temperatures in strained premixed counterflow flames. The C& C model, as described in this work, is now available in the official Cantera release (Goodwin et al. 2024).

Supplementary information The online version contains supplementary material available at https://doi.org/10.1007/s10494-025-00680-5.

Author Contribution T.Z. conducted the investigation, wrote the software, performed the formal analysis, prepared the figures and wrote the original draft. A.K. conceptualized the work, acquired the funding, administrated the project and reviewed and edited the manuscript.

Funding Open Access funding enabled and organized by Projekt DEAL. Funding by the Friedrich und Elisabeth Boysen Stiftung under grant number BOY-195/2 is acknowledged with thanks.

Data Availability Raw data of flame speed calculations are available in the data repository DaRUS (https://doi.org/10.18419/DARUS-5138).

Declarations

Competing Interests The authors declare no competing interests.

References

Alnasif, A., Mashruk, S., Shi, H., Alnajideen, M., Wang, P., Pugh, D., Valera-Medina, A.: Evolution of ammonia reaction mechanisms and modeling parameters: a review. Appl. Energ. Combust. S. **15**, 100175 (2023)

Aniello, A., Laera, D., Berger, L., Attili, A., Poinsot, T.: Introducing thermodiffusive effects in large-eddy simulation of turbulent combustion for lean hydrogen-air flames. In: Center for Turbulence Research, Proceedings of the Summer Program, pp. 267–277. (2022)

ANSYS: ANSYS FLUENT 12.0. Theory Guide. (2009)

Aspden, A., Day, M., Bell, J.: Characterization of low lewis number flames. Proc. Combust. Inst. **33**(1), 1463–1471 (2011)

Bartlett, E.P., Kendall, R.M., Rindal, R.A.: An analysis of the coupled chemically reacting boundary layer and charring ablator. Part 4-A unified approximation for mixture transport properties for multicomponent boundary-layer applications. Technical report, NASA (1968)

Berger, L., Attili, A., Pitsch, H.: Intrinsic instabilities in premixed hydrogen flames: parametric variation of pressure, equivalence ratio, and temperature. part 1-dispersion relations in the linear regime. Combust. Flame **240**, 111935 (2022)

Berger, L., Grinberg, M., Jürgens, B., Lapenna, P.E., Creta, F., Attili, A., Pitsch, H.: Flame fingers and interactions of hydrodynamic and thermodiffusive instabilities in laminar lean hydrogen flames. Proc. Combust. Inst. **39**, 1525–1534 (2023)

Berger, L., Kleinheinz, K., Attili, A., Pitsch, H.: Characteristic patterns of thermodiffusively unstable premixed lean hydrogen flames. Proc. Combust. Inst. **37**, 1879–1886 (2019)
Boivin, P., et al.: Reduced-Kinetic Mechanisms for Hydrogen and Syngas Combustion Including Autoignition. Phd, Universidad Carlos III de Madrid (2011)
Burke, M.P., Chaos, M., Ju, Y., Dryer, F.L., Klippenstein, S.J.: Comprehensive H2/O2 kinetic model for high-pressure combustion. Int. J. Chem. Kinet. **44**(7), 444–474 (2012)
Chai, W.S., Bao, Y., Jin, P., Tang, G., Zhou, L.: A review on ammonia, ammonia-hydrogen and ammonia-methane fuels. Renew. Sustain. Energy Rev. **147**, 111254 (2021)
Chapman, S., Cowling, T.G.: The Mathematical Theory of Non-Uniform Gases. Cambridge university press, Cambridge (1970)
Chen, X., Wang, Y., Zirwes, T., Zhang, F., Bockhorn, H., Chen, Z.: Heat release rate markers for highly stretched premixed CH4/air and CH4/H2/air flames. Energy Fuels **35**(16), 13349–13359 (2021)
Córdoba, O., Arias-Zugasti, M.: Accurate and efficient calculation of multicomponent thermal diffusion coefficients and partial thermal conductivity based on kinetic theory. Combust. Flame **244**, 112202 (2022)
Dinesh, K.R., Shalaby, H., Luo, K., Oijen, J., Thévenin, D.: Effects of pressure on cellular flame structure of high hydrogen content lean premixed syngas spherical flames: a DNS study. Int. J. Hydrogen Energy **41**, 21516–21531 (2016)
Dixon-Lewis, G.: Flame structure and flame reaction kinetics ii. transport phenomena in multicomponent systems. Proc. R. Soc. Lond. Ser. A. Math. And Phys. Sci. **307**(1488), 111–135 (1968)
Eckart, S., Pio, G., Zirwes, T., Zhang, F., Salzano, E., Krause, H., Bockhorn, H.: Impact of carbon dioxide and nitrogen addition on the global structure of hydrogen flames. Fuel **335** (2022)
Gaucherand, J., Laera, D., Schulze-Netzer, C., Poinsot, T.: Intrinsic instabilities of hydrogen and hydrogen/ammonia premixed flames: influence of equivalence ratio, fuel composition and pressure. Combust. Flame **256** (2023)
Gaucherand, J., Laera, D., Schulze-Netzer, C., Poinsot, T.: DNS of turbulent premixed ammonia/hydrogen flames: the impact of thermo-diffusive effects. Flow Turb. Combust. **112**(2), 587–614 (2024)
Girhe, S., Snackers, A., Lehmann, T., Langer, R., Loffredo, F., Glaznev, R., Beeckmann, J., Pitsch, H.: Ammonia and ammonia/hydrogen combustion: comprehensive quantitative assessment of kinetic models and examination of critical parameters. Combust. Flame **267**, 113560 (2024)
Goodwin, D.G., Moffat, H.K., Schoegl, I., Speth, R.L., Weber, B.W.: Cantera: an object-oriented software toolkit for chemical kinetics. Thermodyn., And Transp. Processes (2024). https://www.cantera.org. Ve rsion 3.1.0.
Grcar, J.F., Bell, J.B., Day, M.S.: The Soret effect in naturally propagating, premixed, lean, hydrogen–air flames. Proc. Combust. Inst. **32**(1), 1173–1180 (2009)
Hall, C.A., Pitz, R.W.: Numerical simulation of premixed H2–air cellular tubular flames. Combust. Theory Model **20**(2), 328–348 (2016)
Hirschfelder, J.O., Curtiss, C.F., Bird, R.B.: Molecular Theory of Gases and Liquids, 2nd edn. edn. John Wiley and Sons, Inc., New York, NY (1964)
Howarth, T., Aspden, A.: An empirical characteristic scaling model for freely-propagating lean premixed hydrogen flames. Combust Flame **237**, 111805 (2022)
Howarth, T., Day, M.S., Pitsch, H., Aspden, A.: Thermal diffusion, exhaust gas recirculation and blending effects on lean premixed hydrogen flames. Proc. Comb. Inst. **40**(1–4), 105429 (2024)
Howarth, T., Hunt, E., Aspden, A.: Thermodiffusively-unstable lean premixed hydrogen flames: phenomenology, empirical modelling, and thermal leading points. Combust Flame **253**, 112811 (2023)
Hu, E., Huang, Z., He, J., Zheng, J., Miao, H.: Measurements of laminar burning velocities and onset of cellular instabilities of methane–hydrogen–air flames at elevated pressures and temperatures. Int. J. Hydrogen Energy **34**, 5574–5584 (2009)
Kee, R.J., Coltrin, M.E., Glarborg, P.: Chemically Reacting Flow: theory and Practice. John Wiley & Sons, New York, NY (2005)
Konnov, A.A.: An exploratory modelling study of chemiluminescence in ammonia-fuelled flames. Part 2. Combust Flame **253** (2023)
Kuo, K.K., Acharya, R.: Applications of Turbulent and Multiphase Combustion. John Wiley & Sons, New York (2012)
Lapenna, P.E., Berger, L., Creta, F., Pitsch, H.: Hydrogen laminar flames. In: Hydrogen for Future Thermal Engines, pp. 93–139. Springer, Berlin (2023)
Lapenna, P.E., Lamioni, R., Creta, F.: Subgrid modeling of intrinsic instabilities in premixed flame propagation. Proc. Combust. Inst. **38**(2), 2001–2011 (2021)
Lapenna, P.E., Troiani, G., D'Alessio, F., Creta, F.: Synergistic interplay of thermodiffusive instability and turbulence in premixed flames. Proc. Combust. Inst. **40**(1–4), 105499 (2024)
Law, C., Ishizuka, S., Cho, P.: On the opening of premixed bunsen flame tips. Combust. Sci. Techn. **28**(3–4), 89–96 (1982)

Law, C.K., Jomaas, G., Bechtold, J.K.: Cellular instabilities of expanding hydrogen/propane spherical flames at elevated pressures: theory and experiment. Proc. Combust. Inst. **30**(1), 159–167 (2005)
Lee, H., Dai, P., Wan, M., Lipatnikov, A.N.: A DNS study of extreme and leading points in lean hydrogen-air turbulent flames–part I: local thermochemical structure and reaction rates. Combust Flame **235**, 111716 (2022)
Li, J., Zhao, Z., Kazakov, A., Dryer, F.L.: An updated comprehensive kinetic model of hydrogen combustion. Int. J. Chem. Kinet. **36**, 566–575 (2004)
Lulic, H., Breicher, A., Scholtissek, A., Lapenna, P.E., Dreizler, A., Creta, F., Hasse, C., Geyer, D., Ferraro, F.: On polyhedral structures of lean methane/hydrogen bunsen flames: combined experimental and numerical analysis. Proc. Combust. Inst. (2022)
Neufeld, P.D., Janzen, A., Aziz, R.: Empirical equations to calculate 16 of the transport collision integrals Ω (l, s)* for the Lennard-Jones (12–6) potential. J Chem. Phys **57**(3), 1100–1102 (1972)
Patyal, A., Matalon, M.: Nonlinear development of hydrodynamically-unstable flames in three-dimensional laminar flows. Combust Flame **195**, 128–139 (2018)
Patyal, A., Matalon, M.: Isolating effects of darrieus–Landau instability on the morphology and propagation of turbulent premixed flames. J Fluid Mech **940** (2022)
Paul, P., Warnatz, J.: A re-evaluation of the means used to calculate transport properties of reacting flows. In: Symposium (International) on Combustion, vol. 27, pp. 495–504. Elsevier (1998)
Poling, B.E., Prausnitz, J.M., O'Connell, J.P., et al.: The Properties of Gases and Liquids, vol. 5. Mcgraw-hill New York, New York (2001)
Rieth, M., Gruber, A., Williams, F.A., Chen, J.H.: Enhanced burning rates in hydrogen-enriched turbulent premixed flames by diffusion of molecular and atomic hydrogen. Combust Flame **239** (2022)
Sanders, J.P.H.: Scalar transport and flamelet modelling in turbulent jet diffusion flames. PhD thesis, Eindhoven University of Technology (1994)
Schlup, J., Blanquart, G.: A reduced thermal diffusion model for h and h2. Combust Flame **191**, 1–8 (2018a)
Schlup, J., Blanquart, G.: Validation of a mixture-averaged thermal diffusion model for premixed lean hydrogen flames. Combust. Theory Model **22**, 264–290 (2018b)
Shi, S., Breicher, A., Trabold, J., Hartl, S., Barlow, R.S., Dreizler, A., Geyer, D.: Cellular structures of laminar lean premixed H2/CH4/air polyhedral flames. Appl Energy Combust Sci **13** (2023)
Siemens: Star methodology, version 4.28. Siemens (2017)
Song, W., Perez, F.E.H., Tingas, E.-A., Im, H.G.: Statistics of local and global flame speed and structure for highly turbulent H2/air premixed flames. Combust Flame **232**, 111523 (2021)
Stagni, A., Arunthanayothin, S., Dehue, M., Herbinet, O., Battin-Leclerc, F., Bréquigny, P., Mounaïm-Rousselle, C., Faravelli, T.: Low-and intermediate-temperature ammonia/hydrogen oxidation in a flow reactor: experiments and a wide-range kinetic modeling. Chem. Eng. J. **471**, 144577 (2023)
Sutherland, J., Smith, P., Chen, J.: Quantification of differential diffusion in nonpremixed systems. Combust. Theory Model **9**(2), 365–383 (2005)
Tamadonfar, P., Karimkashi, S., Zirwes, T., Vuorinen, V., Kaario, O.: A numerical study on premixed laminar ammonia/air flames enriched with hydrogen: an analysis on flame–wall interaction. Combust Flame **265**, 113444 (2024)
Tamadonfar, P., Salomaa, V.-P., Rintanen, A., Karimkashi, S., Zirwes, T., Vuorinen, V., Kaario, O.: A numerical study on side-wall quenching of premixed laminar flames: an analysis of ammonia/hydrogen/air mixtures. Combust Flame **275**, 114100 (2025)
Warnatz, J.: Influence of transport models and boundary conditions on flame structure. In: Numerical Methods in Laminar Flame Propagation: a GAMM-Workshop, pp. 87–111. Springer (1982)
Wen, X., Zirwes, T., Scholtissek, A., Böttler, H., Zhang, F., Bockhorn, H., Hasse, C.: Flame structure analysis and composition space modeling of thermodiffusively unstable premixed hydrogen flames–part I: atmospheric pressure. Combust Flame (2021a)
Wen, X., Zirwes, T., Scholtissek, A., Böttler, H., Zhang, F., Bockhorn, H., Hasse, C.: Flame structure analysis and composition space modeling of thermodiffusively unstable premixed hydrogen flames–part II: elevated pressure. Combust Flame (2021b)
Xin, Y., Liang, W., Liu, W., Lu, T., Law, C.K.: A reduced multicomponent diffusion model. Combust Flame **162**(1), 68–74 (2015)
Zhang, F., Zirwes, T., Wang, Y., Chen, Z., Bockhorn, H., Trimis, D., Stapf, D.: Dynamics of premixed hydrogen/air flames in unsteady flow. Phys. Fluids **34**(8) (2022)
Zhang, X., Moosakutty, S.P., Rajan, P.R., Younes, M., Sarathy, S.M.: Combustion chemistry of ammonia/hydrogen mixtures: jet-stirred reactor measurements and comprehensive kinetic modeling. Combust Flame **234**, 111653 (2021)
Zirwes, T., Vignat, G., Toro, E.R., Boigné, E., Younes, K., Trimis, D., Ihme, M.: Improving volume-averaged simulations of matrix-stabilized combustion through direct x-ray μct characterization: application to NH3/H2-air combustion. Combust Flame **257**, 113020 (2023)

Zirwes, T., Zhang, F., Bockhorn, H.: Memory effects of local flame dynamics in turbulent premixed flames. Proc. Combust. Inst. **39**, 2349–2358 (2022)
Zirwes, T., Zhang, F., Wang, Y., Habisreuther, P., Denev, J.A., Chen, Z., Bockhorn, H., Trimis, D.: In-situ flame particle tracking based on barycentric coordinates for studying local flame dynamics in pulsating Bunsen flames. Proc. Combust. Inst. **38**, 2057–2066 (2021)
Zirwes, T., Zhang, F.I., Kaiser, T.L., Oberleithner, K., Stein, O.T., Bockhorn, H., Kronenburg, A.: The role of thermodiffusion and dimensionality in the formation of cellular instabilities in hydrogen flames. Proc. Combust. Inst. **40**(1–4) (2024)